Passive Microwave Remote Sensing of the Antarctic Ice Sheet: Retrieval of Firn Properties Near the Concordia Station

Rahul Kar, *Graduate Student Member, IEEE*, and Mustafa Aksoy, *Member, IEEE*

***Abstract*— This letter discusses the retrieval of important thermal and physical properties of the Antarctic firn via spaceborne microwave radiometry focusing on the Concordia station. Previous studies have indicated that microwave radiometer measurements are sensitive to important properties of the firn from its surface down to deep isothermal ice. Expanding on those work, yearlong Advanced Microwave Scanning Radiometer 2 (AMSR2) and Special Sensor Microwave Imager/Sounder (SSMIS) radiometer measurements over the Concordia station have been used to create brightness temperature spectrograms, i.e., brightness temperatures versus month and frequency, and these spectrograms have been used to retrieve subsurface density and temperature properties of the firn using a plausible forward radiation model. It has been found that utilizing the wide microwave spectrum and long-term measurements, density variations due to internal firn layering, as well as seasonal temperature variations in the near-surface firn can be accurately estimated. In addition, densification of the firn with depth and the deep firn temperature can be retrieved with adequate ancillary data. The results mainly suggest that when deployed with other instruments, such as ground penetrating radars, wideband microwave radiometers can be useful for characterization of ice sheets in future polar remote sensing missions.**

***Index Terms*— Advanced Microwave Scanning Radiometer 2 (AMSR2), Antarctica, Concordia, Global Precipitation Measurement Mission, ice sheets, microwave radiometry, polar firn, remote sensing, Special Sensor Microwave Imager/Sounder (SSMIS).**

I. Introduction

UNDERSTANDING the physics and dynamics of Earth's cryosphere is important for predicting future changes in its ice volume and mass, which are critical to track the climate and water cycle on our planet [1], [2]. Because of the extreme environmental conditions, high costs of sparse in situ measurements, and concerns about increasing human footprint associated with these regions, remote sensing instruments are commonly used to monitor the cryosphere [3]. Among all remote sensing systems, microwave radiometers, i.e., passive receivers measuring microwave radiation from their targets, are particularly useful for cryosphere observations as they can provide measurements irrespective of solar illumination and cloud conditions, and their measurements are highly sensitive to important subsurface properties of the polar firn [4], [5]. These instruments with enough bandwidth are hypothetically able to profile firn properties from surface down to deep ice by utilizing electromagnetic emission models with plausible models for depth-dependent physical and thermal properties of ice [6], [7], [8]. As the electromagnetic penetration depth in ice changes with frequency, different frequency channels of wideband radiometers are sensitive to different depths. A previous study has demonstrated how the global precipitation measurement (GPM) constellation can be used as a multifrequency (ten frequency channels at 6.9, 7.3, 10.65, 18.7, 19.35, 23.8, 36.5, 37, 89, and 91.665 GHz) microwave radiometer system to characterize the Antarctic firn in terms of its physical and thermal properties, such as firn temperature, density, and grain size [9]. Expanding upon that study, this letter presents a comprehensive retrieval procedure for Antarctic firn properties using yearlong wideband radiometer measurements focusing on the Concordia station. Intercalibrated brightness temperature measurements of the Advanced Microwave Scanning Radiometer 2 (AMSR2) and the Special Sensor Microwave Imager/Sounder (SSMIS) [10] in the GPM constellation at eight frequencies as well as the 6.9- and 7.3-GHz brightness temperature measurements of AMSR2 have been collected from 2020 to 2021 and averaged monthly over a 0.25° × 0.25° latitude–longitude grid cell centered around the Concordia (75°05′ 59"S 123°19′ 56"E) station, resulting in brightness temperature spectrograms in both horizontal and vertical polarizations. Standard deviations of the same data for each month and frequency were also calculated to create associated standard deviation spectrograms. Fig. 1 depicts the vertically polarized brightness temperature and standard deviation spectrograms. This work, using these brightness temperature spectrograms, is the first attempt to retrieve the depth-dependent density and internal temperature profiles of the Antarctic firn near the Concordia station with the overarching goal to reach cost-effective, convenient, and accurate long-term observations of the whole Antarctic system via microwave radiometry. Section II describes the microwave emission model used in this study, Section III explains the retrieval study, and Sections IV and V discuss the research results and conclusions.

II. Radiation Model

A simple microwave emission model has been developed, where the brightness temperatures at the firn surface at

Manuscript received 15 June 2023; revised 5 December 2023; accepted 12 December 2023. Date of publication 15 December 2023; date of current version 28 December 2023. This work was supported by the National Science Foundation under Grant 1844793 and Grant 2143592. *(Corresponding author: Rahul Kar.)*

The authors are with the Department of Electrical and Computer Engineering, University at Albany, State University of New York, Albany, NY 12222 USA (e-mail: rkar@albany.edu; maksoy@albany.edu).

Digital Object Identifier 10.1109/LGRS.2023.3343594

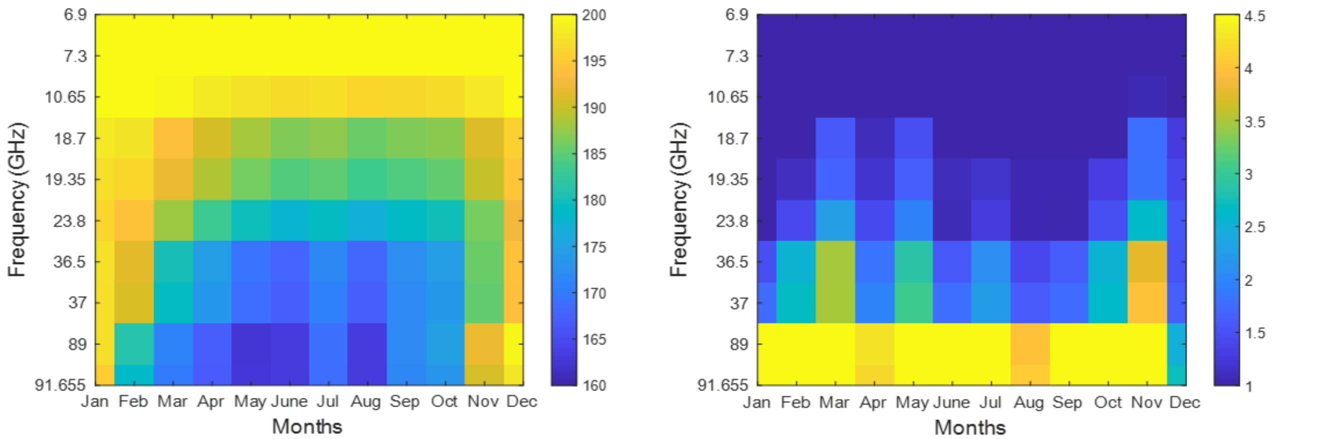

Fig. 1. (Left) Vertically polarized brightness temperature and (right) standard deviation spectrograms generated using AMSR2 and SSMIS measurements from 2020 to 2021 over the Concordia station in Antarctica.

frequency f, $T_B(z=0, f)$ are calculated analytically using a zeroth-order radiative transfer equation as described in [9]

$$T_B(z=0, f, \theta_i, p) = \int_{z_{\text{deep}}}^{z=0} \left[\prod_{z'=z}^{z'=0} \Gamma\left(z', \theta\left(z'\right), p\right)\right] \kappa_e(f, z) \sec\theta(z) \times T(z) e^{-\int_{z'=z}^{z'=0} \kappa_e\left(z', f\right) \sec\theta\left(z'\right) dz'} dz \tag{1}$$

where $\Gamma\left(z', \theta\left(z'\right), p\right)$, $\theta\left(z'\right)$, and $T(z)$ are the amplitude squared of the Fresnel transmission coefficient at the ice layer interface at depth z' for polarization p, the angle of incidence at the ice layer interface at depth z', and the physical firn temperature at depth z, respectively. κ_e is the extinction coefficient. The top of the atmosphere brightness temperatures measured by the spaceborne radiometers is

$$T_{B_{\text{toa}}}(f) = T_B(z=0, f) \times K(f) + T_{B_{\text{atm}}}(f) \tag{2}$$

where $K(f)$ and $T_{B_{\text{atm}}}(f)$ are the atmospheric attenuation factor and the atmospheric brightness temperature contribution at frequency f, respectively. These terms have been computed based on the ITU recommendations for standard atmosphere expressions [11] and further corrected using the available polar radiosonde data [12].

Note that the extinction coefficients in (1) have been found using the Microwave Emission Model of Layered Snowpacks (MEMLSs) [13], and they, along with the transmission coefficients and firn temperatures, are calculated using the following parametric models for the physical and thermal properties of the Antarctic firn to compute the surface brightness temperatures, $T_B(z=0, f)$. This radiation model was used to simulate the vertically polarized brightness temperature and standard deviation spectrograms shown in Fig. 2.

A. Firn Density

The density profile versus depth, $\rho(z)$, is described as the sum of a smooth average firn density and random fluctuations due to internal layering as presented in [14]

$$\rho(z) = \rho_\infty - (\rho_\infty - \rho_0) e^{-z/\beta} + \rho_n(z) e^{-z\alpha} \ \text{kg/m}^3 \tag{3}$$

where ρ_0 is the near surface density, ρ_∞ is the compacted ice density in deep ice, z is the depth, and β is a factor that controls densification. $\rho_n(z)$ is a zero-mean Gaussian noise, which represents the fluctuations associated with internal layering. These fluctuations are damped with depth according to the damping factor α. The values of ρ_∞ and ρ_0 are taken as 922 and 336 kg/m^3, respectively; and the standard deviation of the noise is assumed to be 50 kg/m^3 based on previous density measurements near the Concordia station [15], [16].

B. Grain Radius

Antarctic firn grain size profile versus depth, $r(z)$, is modeled based on in situ measurements as described in [17]

$$r(z) = \sqrt{r_o^2 + z \times g_r} \ \text{m} \tag{4}$$

where r_o is the grain radius at the surface in meters, g_r is the grain size gradient in square meter per meters, and z is the depth in meters. A least-squares fitting to the in situ grain size measurements near the Concordia station [18], [19] plotted in Fig. 3 has led to $r_o = 0.57 \times 10^{-3}$ m and $g_r = 5.07 \times 10^{-9}$ m^2/m, which is used in this study. In addition, as described in [20], to achieve a better match between radiation simulations and the spaceborne radiometer measurements, the grain radius at the surface, r_o, has been multiplied with an empirical snow grain size scaling factor Φ, whose value varies between 0 and 5 across the entire frequency range. The values of Φ identified in this study are given in Fig. 4 at all AMSR2 and SSMIS frequencies.

The resulting grain size profile, therefore, is as follows:

$$r(z) = \sqrt{\left(\Phi \times 0.57 \times 10^{-3}\right)^2 + z \times \left(5.07 \times 10^{-9}\right)} \ \text{m}. \tag{5}$$

C. Internal Temperature

In this study, internal firn temperature versus depth, $T(z)$, has been approximated as the sum of a constant isothermal deep ice temperature and sinusoidal near-surface variations representing the seasonal changes. The weights of these two components are assumed to decay exponentially toward the surface and deep ice; and the overall temperature profile is modeled as

$$T(z) = T_{\text{iso}} \times \left(1 - e^{-z \times T_{\text{atten}}}\right) + T_{\sin} \times e^{-z \times T_{\text{atten}}} \tag{6}$$

where the boundaries of the near surface fluctuations, $T_{\sin}$, are taken to be 239.9 and 209.6 K, respectively, based on previous

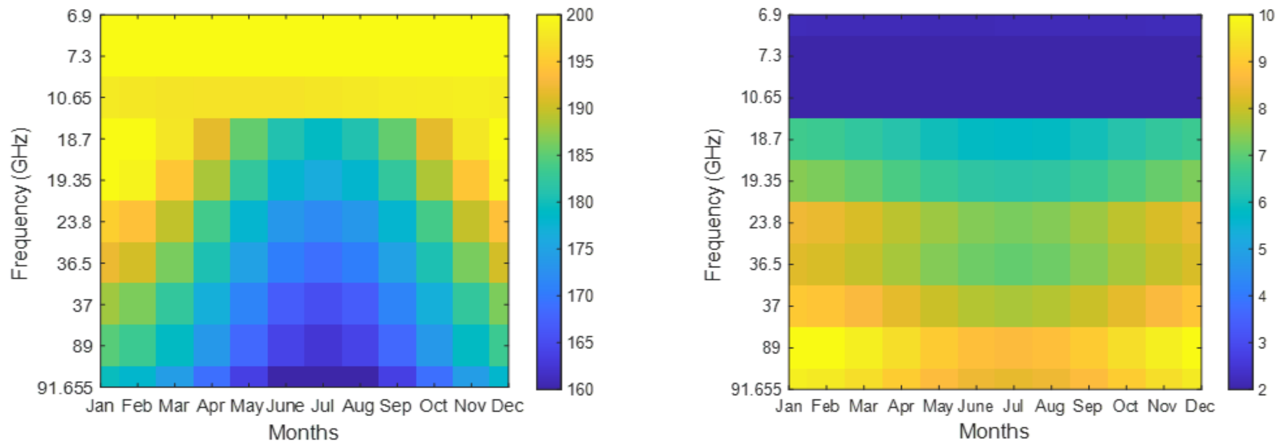

Fig. 2. (Left) Vertically polarized brightness temperature and (right) standard deviation spectrograms simulated using the radiation model discussed in Section II and picked by the retrieval algorithm for the Concordia station.

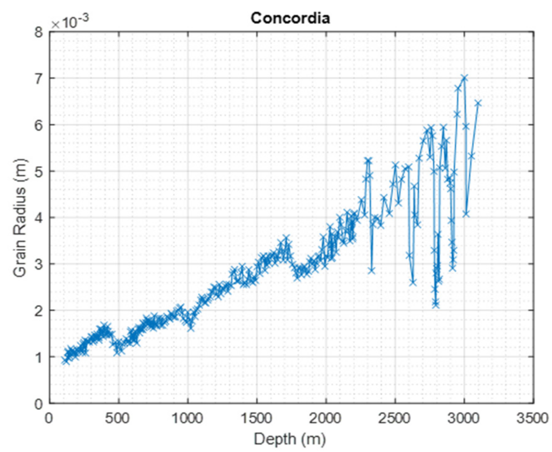

Fig. 3. In situ measurements of grain size versus depth near the Concordia station in Antarctica [18].

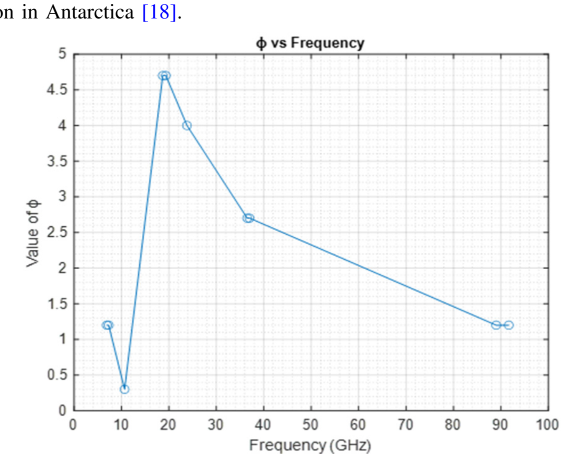

Fig. 4. Value of Φ varying across the entire frequency range.

in situ measurements [21]. Its spatial period, on the other hand, is left variable.

III. Retrieval Process

The retrieval algorithm takes measured brightness temperature spectrograms, i.e., brightness temperatures measured by AMSR2 and SSMIS versus month and frequency, as shown in Fig. 1, as inputs and compare them with a set of simulated spectrograms generated using the radiation model described in Section II by varying the density and temperature-related firn parameters in (3) and (6). Table I demonstrates the maximum and minimum values of these density and temperature variables as well as the variation resolutions considered in this study. The boundaries are set based on in situ measurements at several locations in the Antarctic Ice Sheet [14], and 100 brightness temperatures have been generated for each set of firn parameters for each month and frequency. Their average and standard deviations have been computed as simulated brightness temperature and standard deviation spectrograms. Then, through a least squares analysis, closest simulations to the measured brightness temperature spectrograms are found, and the ice parameters used to simulate those spectrograms are outputted as retrieved firn properties. The least-squares procedure includes taking the difference between simulated and measured brightness temperature spectrograms and dividing the squared differences by the measured standard deviation spectrograms. The results are averaged over month and frequency, and these single error values are used for the retrieval.

TABLE I

Ice Parameters to be Retrieved and Their Maximum and Minimum Possible Values Considered in This Study

Parameter	**Min Value**	**Max Value**	**Resolution**
β	10 m	70 m	10 m
α	0 m^{-1}	0.1 m^{-1}	0.01 m^{-1}
T_{iso}	200 K	250 K	5 K
T_{atten}	0.2 m^{-1}	0.5 m^{-1}	0.05 m^{-1}
Period of T_{sin}	5 m	15 m	2 m

IV. Results

As mentioned before, Fig. 2 depicts the simulated brightness temperature and the standard deviation spectrograms picked by the retrieval process for the Concordia station. These spectrograms are the result of the radiation model using the firn parameter values given in Table II, and Fig. 5 shows the density and subsurface temperature profiles created by using these values in (3) and (6). The table also provides the values of the same firn parameters extracted from previous in situ measurements [16], [21]. While α and the spatial period of T_{sin} are retrieved accurately considering the resolution of changes in the firn parameter values shown in Table I,

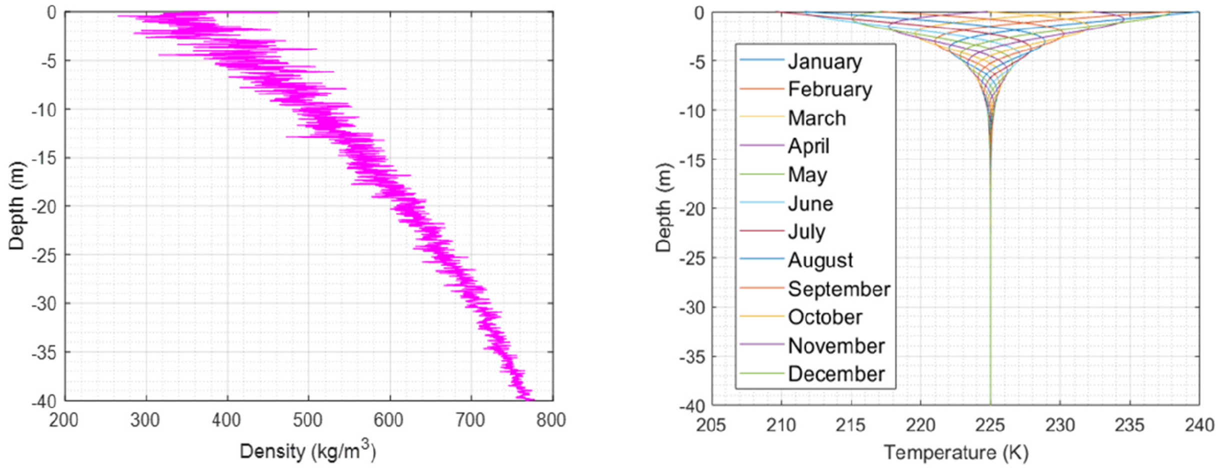

Fig. 5. (Left) Firn density and (right) temperature profiles versus depth created using (3) and (6) with the retrieved firn parameters for the Concordia station.

TABLE II

RETRIEVED FIRN PARAMETER VALUES FOR THE CONCORDIA STATION AND THE AVAILABLE IN SITU MEASUREMENTS

Parameter	**Retrieved Value**	**In-Situ Value**
β	30 m	50 m
α	0.05 m^{-1}	0.05 m^{-1}
T_{iso}	225 K	218 K
T_{atten}	0.4 m^{-1}	0.5 m^{-1}
Period of T_{sin}	9 m	10 m

there are slight errors in other parameter values. Especially the underestimation of β and the overestimation of deep ice temperature would wrongfully imply rapid densification with depth and higher geothermal heat flux. To investigate these errors, brightness temperature spectrograms have also been calculated with the true firn parameters and the errors between simulated and measured spectrograms have been analyzed. The average error for the retrieval, as described in Section III, is 2.06, whereas this value would be 2.29 if the in situ firn parameters were used for the simulations. Thus, it is concluded that the difference between the retrieved and in situ firn parameter values is so small that, i.e., 0.23 standard deviations in average, the retrievals may not be unique. Different sets of firn parameter values may lead to similar brightness temperature spectrograms, ramifications of which are discussed in Section V.

V. CONCLUSION

This letter presents the first attempt of retrieving polar firn properties using wideband microwave radiometer measurements at frequencies from C-band to W-band. Focusing on the Concordia station of the Antarctic Ice sheet, the intercalibrated measurements of the AMSR2 and SSMIS radiometers at frequencies from 10.65 to 91.665 GHz as well as 6.9- and 7.3-GHz measurements of AMSR2 for one year have been used to estimate the subsurface density and temperature profiles of the Antarctic firn. Utilizing the wide spectrum and seasonal variations throughout the year, the densification factor, density fluctuation rate due to internal firn layering, deep firn temperature, damping rate of seasonal temperature variations with respect to depth, and the spatial period of such variations have been retrieved. Retrieval results, overall, match with in situ measurements available in the literature, with nonnegligible errors in firn densification and deep firn temperature parameters. However, it has been found that these errors are mainly due to the nonuniqueness of the retrieval process as both retrieved and in situ firn parameters yield to similar brightness temperature spectrograms. This is an important result suggesting that ancillary data may be needed for passive microwave remote sensing of the polar ice sheets. Constraining the density parameters with ground penetrating radar measurements or thermal properties using in situ heat flow measurements may remove the problem of nonuniqueness in the retrieval process.

Future studies will focus on utilizing such ancillary data as well as incorporation of the 6.9- and 7.3-GHz measurements into the intercalibration process for more accurate retrievals of firn parameters via microwave radiometry. Also, wider geographic regions and a more inclusive set of ice parameters will be considered for a comprehensive analysis. Finally, based on the analyses result, radiometer designs and deployment scenarios will be suggested for future polar remote sensing missions.

ACKNOWLEDGMENT

The AMSR2 and SSMIS data were obtained from the NASA Goddard Space Flight Center's Precipitation Processing System (PPS) [22] and the Globe Portal System (G-Portal) of JAXA [23].

REFERENCES

[1] M. Aksoy et al., "An examination of multi-frequency microwave radiomtry for probing subsurface ice sheet temperature," in *Proc. IEEE Geosci. Remote Sens. Symp.*, Quebec City, QC, Canada, Jul. 2014, pp. 3614–3617.

[2] S. Solomon, M. Manning, M. Marquis, and D. Quin, *Climate Change 2007—The Physical Science Basis*, document AR4, Working Group I Contribution to the Fourth Assessment Report of the IPCC, Cambridge Univ. Press, Cambridge, U.K., 2007.

[3] G. Picard, A. Royer, L. Arnaud, and M. Fily, "Influence of meter-scale wind-formed features on the variability of the microwave brightness temperature around Dome C in Antarctica," *Cryosphere*, vol. 8, no. 3, pp. 1105–1119, Jun. 2014.

[4] J. Turner et al., "Antarctic climate change during the last 50 years," *Int. J. Climatol.*, vol. 25, no. 3, pp. 279–294, 2005.

[5] E. J. Steig, D. P. Schneider, S. D. Rutherford, M. E. Mann, J. C. Comiso, and D. T. Shindell, "Warming of the Antarctic ice-sheet surface since the 1957 international geophysical year," *Nature*, vol. 457, no. 7228, pp. 459–462, Jan. 2009, doi: 10.1038/nature07669.

[6] K. C. Jezek et al., "Radiometric approach for estimating relative changes in intraglacier average temperature," *IEEE Trans. Geosci. Remote Sens.*, vol. 53, no. 1, pp. 134–143, Jan. 2015.

[7] Y. Duan et al., "Testing the feasibility of a Bayesian retrieval of Greenland ice sheet internal temperature from ultra-wideband software-defined microwave radiometer (UWBRAD) measurements," in *Proc. IEEE Int. Geosci. Remote Sens. Symp. (IGARSS)*, Beijing, China, Jul. 2016, pp. 7092–7093.

[8] J. T. Johnson et al., "The ultra-wideband software-defined radiometer (UWBRAD) for ice sheet internal temperature sensing: Results from recent observations," in *Proc. IEEE Int. Geosci. Remote Sens. Symp. (IGARSS)*, Beijing, China, Jul. 2016, pp. 7085–7087.

[9] R. Kar, M. Aksoy, D. Kaurejo, P. Atrey, and J. A. Devadason, "Antarctic firn characterization via wideband microwave radiometry," *Remote Sens.*, vol. 14, no. 9, p. 2258, May 2022.

[10] W. Berg et al., "Intercalibration of the GPM microwave radiometer constellation," *J. Atmos. Ocean. Technol.*, vol. 33, no. 12, pp. 2639–2654, Dec. 2016.

[11] *Recommendation ITU-R P.835-6. Attenuation by Atmospheric Gases*. Accessed: Jul. 15, 2020. [Online]. Available: https://www.itu.int/dms_pubrec/itu-r/rec/p/R-REC-P.835-6-201712-I!!PDF-E.pdf

[12] C. Tomasi, B. Petkov, E. Benedetti, L. Valenziano, and V. Vitale, "Analysis of a 4 year radiosonde data set at Dome C for characterizing temperature and moisture conditions of the Antarctic atmosphere," *J. Geophys. Res.*, vol. 116, no. 15, 2011, Art. no. D15304.

[13] M. Proksch et al., "MEMLS3&a: Microwave emission model of layered snowpacks adapted to include backscattering," *Geosci. Model Develop.*, vol. 8, no. 8, pp. 2611–2626, Aug. 2015.

[14] D. Kaurejo, M. Aksoy, and R. Kar, "Analysis of polar firn density and grain size models using available data," in *Proc. IEEE Int. Geosci. Remote Sens. Symp. (IGARSS)*, Malaysia, Jul. 2022, pp. 3987–3990.

[15] R. B. Alley, J. F. Bolzan, and I. M. Whillans, "Polar firn densification and grain growth," *Ann. Glaciol.*, vol. 3, pp. 7–11, Jan. 2017.

[16] M. Leduc-Leballeur et al., "Modeling L-band brightness temperature at Dome C in Antarctica and comparison with SMOS observations," *IEEE Trans. Geosci. Remote Sens.*, vol. 53, no. 7, pp. 4022–4032, Jul. 2015.

[17] L. Brucker, G. Picard, and M. Fily, "Snow grain-size profiles deduced from microwave snow emissivities in Antarctica," *J. Glaciol.*, vol. 56, no. 197, pp. 514–526, 2010.

[18] G. Durand and J. Weiss, *EPICA Dome C Ice Cores Grain Radius Data*, document 2004-039, IGBP PAGES/World Data Center for Paleoclimatology Data Contribution Series, NOAA/NGDC Paleoclimatology Program, Boulder, CO, USA, 2004.

[19] I. Baker and R. Obbard, "Microstructural location and composition of impurities in polar ice cores," Nat. Snow Ice Data Center (NSIDC), U.S. Antarctic Program (USAP) Data Center, Boulder, CO, USA, Tech. Rep., Feb. 2010. [Online]. Available: http://www.usap-dc.org/view/dataset/609436, doi: 10.7265/N5DF6P5P.

[20] G. Picard et al., "Simulation of the microwave emission of multi-layered snowpacks using the dense media radiative transfer theory: The DMRT-ML model," *Geosci. Model Develop.*, vol. 6, no. 4, pp. 1061–1078, Jul. 2013.

[21] L. Brucker et al., "Modeling time series of microwave brightness temperature at Dome C, Antarctica, using vertically resolved snow temperature and microstructure measurements," *J. Glaciol.*, vol. 57, no. 201, pp. 171–182, 2011.

[22] *Precipitation Processing System*. Accessed: Jul. 18, 2021. [Online]. Available: https://pps.gsfc.nasa.gov/

[23] *G-Portal, Globe Portal System*. Accessed: Jul. 11, 2021. [Online]. Available: https://gportal.jaxa.jp/gpr/?lang=en